Search for spin-3/2 quarks at the Large Hadron Collider

Duane A. Dicus, Durmus Karabacak, S. Nandi, and Santosh Kumar Rai

Phys. Rev. D **87**, 015023 — Published 22 January 2013

DOI: 10.1103/PhysRevD.87.015023

OSU-HEP-12-10

Search for spin–3/2 quarks at the Large Hadron Collider

Duane A. Dicus[1,*], Durmus Karabacak[2,†], S. Nandi[2,‡], and Santosh Kumar Rai[2,§]

[1] *Department of Physics,*

University of Texas,

Austin TX 78712-1081, USA

[2] *Department of Physics and Oklahoma Center for High Energy Physics,*

Oklahoma State University,

Stillwater OK 74078-3072, USA

We consider the pair production of color triplet spin–$\frac{3}{2}$ quarks and their subsequent decays at the LHC. This particle, if produced, will most likely decay into top quark and gluon, bottom quark and gluon, or a light quark jet and gluon, depending on the quantum number of the spin–$\frac{3}{2}$ particle. This would lead to signals with $t\bar{t}jj$, $b\bar{b}jj$, or $4j$ in the final states. We present a detailed analysis of the signals and backgrounds at $\sqrt{s}$ = 7, 8 and 14 TeV and show the reach for such particles by solving for observable mass values for the spin–$\frac{3}{2}$ quarks through its decay products.

I. INTRODUCTION

The Standard Model (SM) of particle physics has been extensively tested by many independent experiments and the results are in agreement with the predictions of the SM. The Large Hadron Collider (LHC) at CERN is designed to explore the energy and intensity frontier which could show physics beyond the SM. The initial results released by the ATLAS and CMS experiments not only confirm the predictions of the SM, including the discovery of the Higgs boson [1, 2], but have also started pushing the energy scale required by new physics models including exotic fermions and gauge bosons which are not present in the SM. Among exotic fermions one possible new particle is a spin–$\frac{3}{2}$ excitation of quarks. We will assume this spin–$\frac{3}{2}$ particle to be a color triplet like an ordinary quark and consider the pair

* Electronic address: dicus@physics.utexas.edu
† Electronic address: durmas@ostatemail.okstate.edu
‡ Electronic address: s.nandi@okstate.edu
§ Electronic address: santosh.rai@okstate.edu

production and the decay of such an exotic particle at the LHC.

It is not outside the realm of possibility that a spin–$\frac{3}{2}$ quark could exist as a fundamental particle. We could also have spin–$\frac{3}{2}$ bound states of ordinary quarks with gluons or the Higgs boson. There are also theoretical models in which spin–$\frac{3}{2}$ quarks arise as bound states of three heavy quarks for sufficiently strong Yukawa couplings [3]. The masses of these bound states are typically expected to be a few TeV. A heavy spin–$\frac{3}{2}$ quark could also exist as the lightest Regge recurrences of light spin–$\frac{1}{2}$ quarks or as Kaluza-Klein modes in string theory if one or more of the compactification radii is of the order of the weak scale rather than the Planck scale and such weak compactification in the framework of both string theory and field theory has been popular [4]. In this work we restrict ourselves to the collider production of point-like spin–$\frac{3}{2}$ color triplet quarks. The production of spin–$\frac{3}{2}$ quarks by hadronic collisions has been previously considered by Moussallam and Soni [5] and by Dicus, Gibbons, and Nandi [6]. There are several studies on production of spin–$\frac{3}{2}$ fermions at lepton colliders [7–9] and also the virtual effects of such particles on $t\bar{t}$ production [10].

Our paper is organized as follows. In Section II, we give the Feynman rules relevant for the production of spin–$\frac{3}{2}$ quarks. In Section III, we give the explicit analytic formulae for the squares of the amplitude, various subprocess cross sections and total production cross sections. In Section IV, we present the analysis of the signal of spin–$\frac{3}{2}$ particle decaying into light jets or into heavy flavor modes. Here we make the physics analysis of relevant background and signal for three different decay scenarios. Section V contains a summary.

II. FEYNMAN RULES FOR SPIN–$\frac{3}{2}$ PARTICLES

The Lagrangian and the equations of motion for a free spin–$\frac{3}{2}$ particle of mass M can be written as [11, 12]

$$\mathcal{L} = \bar{\psi}_\alpha \Lambda^{\alpha\beta} \psi_\beta \tag{2.1}$$

$$\Lambda^{\alpha\beta}\psi_\beta = 0 \tag{2.2}$$

where

$$\Lambda_{\alpha\beta} = (i\partial\!\!\!/ - M) g_{\alpha\beta} + iA(\gamma_\alpha \partial_\beta + \gamma_\beta \partial_\alpha) + \frac{iB}{2}\gamma_\alpha \partial\!\!\!/ \gamma_\beta + CM\gamma_\alpha\gamma_\beta \tag{2.3}$$

with $B \equiv 3A^2 + 2A + 1$ and $C \equiv 3A^2 + 3A + 1$. The parameter A is arbitrary except that $A \neq -\frac{1}{2}$. The field ψ_α satisfies the subsidiary conditions

$$\gamma^\alpha \psi_\alpha = 0 \tag{2.4}$$

$$\partial^\alpha \psi_\alpha = 0. \tag{2.5}$$

The propagator $S_{\alpha\beta}$ is given by

$$\begin{aligned} S_{\alpha\beta}(p) =& \frac{1}{\not{p} - M}\left[g_{\alpha\beta} - \frac{1}{3}\gamma_\alpha\gamma_\beta - \frac{2}{3M^2}p_\alpha p_\beta + \frac{1}{3M}(p_\alpha\gamma_\beta - p_\beta\gamma_\alpha)\right] \\ &+ \left\{\frac{a^2}{6M^2}\not{p}\gamma_\alpha\gamma_\beta - \frac{ab}{3M}\gamma_\alpha\gamma_\beta + \frac{a}{3M^2}\gamma_\alpha p_\beta + \frac{ab}{3M^2}\gamma_\beta p_\alpha\right\} \end{aligned} \tag{2.6}$$

where

$$a = \frac{A+1}{2A+1} \quad \text{and} \quad b = \frac{A}{2A+1} \quad .$$

From Eq.(2.4) and Eq.(2.5) the terms depending on the parameter A in the propagator vanish on the mass shell. A redefinition of the spin–$\frac{3}{2}$ field ψ_α allows one to remove the A dependent terms in the propagator [13]. However, in our analysis we have kept the A dependence in the propagator and in the interaction vertices and used the disappearance of A as a check on our calculations.

The minimal substitution in Eq.(2.1) gives the interaction of spin–$\frac{3}{2}$ quarks with gluon and photon fields,

$$\mathcal{L}_I = g\bar{\psi}_\alpha\left(\frac{B}{2}\gamma^\alpha\gamma^\mu\gamma^\beta + Ag^{\alpha\mu}\gamma^\beta + A\gamma^\alpha g^{\mu\beta} + g^{\beta\alpha}\gamma^\mu\right)T_a\psi_\beta A^a_\mu \ , \tag{2.7}$$

where g is the coupling constant, T_a's are the group generators and A^a_μ are the gauge fields. For on-shell particles only the last term is nonzero.

III. CALCULATION OF CROSS SECTIONS

In this section we provide the expressions necessary for the process,

$$p\ p \to Q_{3/2}\ \bar{Q}_{3/2} \tag{3.1}$$

where $Q_{3/2}$ is the spin–$\frac{3}{2}$ quark. There are two subprocesses which contribute, $q\bar{q}$ annihilation and gluon fusion. The Feynman diagrams are shown in Fig.1 where *(a)* represents the $q\bar{q}$

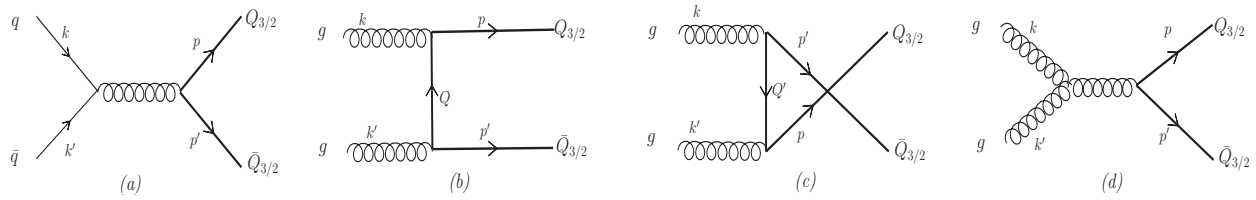

FIG. 1: *The leading order (LO) Feynman diagrams for the pair production of spin–$\frac{3}{2}$ quarks through (a) $q\bar{q}$ and gg initial states in (b) t-channel, (c) u-channel and (d) s-channel.*

annihilation while *(b)–(d)* represent the t,u and s-channel contributions of the gluon fusion subprocess respectively. Just as for top quark production the largest contribution to the production of spin–$\frac{3}{2}$ at LHC energies is through gluon fusion.

The t-channel amplitude shown in Fig.1 is given by

$$\begin{aligned}\mathcal{M}_t = \; & g_s^2 \bar{u}_\rho(p)\big(g^{\rho\alpha}\gamma^\mu + A g^{\mu\rho}\gamma^\alpha\big)T_a\epsilon^a_\mu(k) \\ & \left\{\frac{1}{\not{Q}-M}\left[g_{\alpha\beta} - \frac{1}{3}\gamma_\alpha\gamma_\beta - \frac{2}{3M^2}Q_\alpha Q_\beta + \frac{1}{3M}\big(Q_\alpha\gamma_\beta - Q_\beta\gamma_\alpha\big)\right]\right. \\ & \left. + \frac{a^2}{6M^2}\not{Q}\gamma_\alpha\gamma_\beta - \frac{ab}{3M}\gamma_\alpha\gamma_\beta + \frac{a}{3M^2}\gamma_\alpha Q_\beta + \frac{ab}{3M^2}\gamma_\beta Q_\alpha\right\} \\ & \big(g^{\sigma\beta}\gamma^\nu + A g^{\nu\sigma}\gamma^\beta\big)T_b\epsilon^b_\nu(k')v_\sigma(p') \quad ,\end{aligned} \tag{3.2}$$

while the u channel amplitude has a similar form due to crossing symmetry,

$$\begin{aligned}\mathcal{M}_u = \; & g_s^2 \bar{u}_\rho(p)\big(g^{\rho\beta}\gamma^\nu + A g^{\rho\nu}\gamma^\beta\big)T_b\epsilon^b_\nu(k') \\ & \left\{\frac{1}{\not{Q}^{'}-M}\left[g_{\beta\alpha} - \frac{1}{3}\gamma_\beta\gamma_\alpha - \frac{2}{3M^2}Q^{'}_\beta Q^{'}_\alpha + \frac{1}{3M}\big(Q^{'}_\beta\gamma_\alpha - Q^{'}_\alpha\gamma_\beta\big)\right]\right. \\ & \left. + \frac{a^2}{6M^2}\not{Q}^{'}\gamma_\beta\gamma_\alpha - \frac{ab}{3M}\gamma_\beta\gamma_\alpha + \frac{a}{3M^2}\gamma_\beta Q^{'}_\alpha + \frac{ab}{3M^2}\gamma_\alpha Q^{'}_\beta\right\} \\ & \big(g^{\sigma\alpha}\gamma^\mu + A g^{\sigma\mu}\gamma^\alpha\big)T_a\epsilon^a_\mu(k)v_\sigma(p') \,,\end{aligned} \tag{3.3}$$

where $\not{Q} = \not{p} - \not{k}$, $\not{Q}' = \not{k} - \not{p}'$. The amplitude for the s-channel contribution has a much simpler form because the A dependence goes away for the spin–$\frac{3}{2}$ particles produced on-shell,

$$\begin{aligned}\mathcal{M}_s = & -ig_s^2 f_{abc}\bar{u}^\rho(p)\gamma^\alpha T^c v_\rho(p')\frac{1}{\hat{s}}\epsilon^a_\mu(k)\epsilon^b_\nu(k') \\ & \left[g^{\mu\alpha}(2k+k^{'})^\nu - g^{\alpha\nu}(2k^{'}+k)^\mu + g^{\nu\mu}(k^{'}-k)^\alpha\right] .\end{aligned} \tag{3.4}$$

The ϵ^a's represent the gluon fields while the spin–$\frac{3}{2}$ particles are denoted by the u and v spinors carrying Lorentz indices. From the expressions $\mathcal{M}_t$ and $\mathcal{M}_u$ we see that off-shell spin–$\frac{3}{2}$ particle exchange leads to an explicit dependence on the contact parameter A. Although we have this dependence in the amplitudes, the final results should be independent of A. Indeed, we find that this dependence goes away not only from the final total result but also from each individual contribution such as $\Sigma|\mathcal{M}_t|^2$ or $\Sigma|\mathcal{M}_u|^2$ or the cross terms. This was verified by calculating the amplitude squares and all interference terms in both axial-gauge and Feynman-gauge.

Using Eqs.(3.2-3.4), the full spin and color averaged matrix amplitude square for the gluon-gluon subprocess is

$$\begin{aligned}\sum|\mathcal{M}|^2_{GG} \;=\; & \frac{g_s^4}{1944}\left[-2106-\frac{5832M^2}{\hat{s}}+\frac{112\hat{s}}{M^2}-\frac{272\hat{s}^2}{M^4}+\frac{39\hat{s}^3}{M^6}-\frac{2592M^4\hat{s}^2}{u'^2t'^2}-\frac{48\hat{s}^4}{u'^2t'^2}\right.\\ & +\frac{5832M^4}{u't'}+\frac{2592M^2\hat{s}}{u't'}+\frac{539\hat{s}^2}{u't'}+\frac{4\hat{s}^3}{M^2u't'}+\frac{33\hat{s}^4}{M^4u't'}+\frac{521u't'}{M^4}+\frac{2916u't'}{\hat{s}^2}\\ & \left.-\frac{121\hat{s}u't'}{M^6}+\frac{4\hat{s}^2u't'}{M^8}-\frac{8u'^2t'^2}{M^8}\right] \end{aligned} \tag{3.5}$$

where t' and u' are related to the usual definitions of the Mandelstam variables t and u in the parton center-of-mass frame as $t'=t-M^2$ and $u'=u-M^2$. The total cross section for the gluon-gluon subprocess is then

$$\begin{aligned}\hat{\sigma}(gg\to Q_{3/2}\bar{Q}_{3/2}) =& \frac{\pi\alpha_s^2}{116640\ \hat{s}}\left\{60\ \ln\left(\frac{1+\beta}{1-\beta}\right)\left[66y^2+8y+886+5184\frac{1}{y}+1296\frac{1}{y^2}\right]\right.\\ & \left.+\beta\left[24y^4+1178y^3-13626y^2+11380y-97200-602640\frac{1}{y}\right]\right\}\end{aligned} \tag{3.6}$$

where $\alpha_s\equiv g_s^2/4\pi$, $y\equiv\hat{s}/M^2$ and $\beta\equiv\sqrt{1-4/y}$. This expression for the total subprocess cross section agrees with Ref.[6], but disagrees with Ref.[5]. However Ref.[5] has an algebraic error which, when corrected, gives agreement with Eq.(3.6) [14].

The pair production of the spin–$\frac{3}{2}$ quarks will also have contributions coming from the amplitude for the quark-antiquark annihilation subprocess which is given by

$$\mathcal{M}_{q\bar{q}}=-ig^2\frac{1}{\hat{s}}\bar{u}^\rho(p)T_a\gamma^\mu v_\rho(p')\bar{u}(k)\gamma_\mu v(k')\ . \tag{3.7}$$

The spin and color averaged matrix amplitude square for the quark-antiquark process is

$$\begin{aligned}\sum|\mathcal{M}_{q\bar{q}}|^2 \;=\; & \frac{4g_s^4}{81M^4\hat{s}^2}\left[36\hat{s}M^6-2\hat{s}M^2(\hat{s}+2t')^2+\hat{s}^2(\hat{s}^2+2\hat{s}t'+2t'^2)\right.\\ & \left.+2M^4(\hat{s}^2+18\hat{s}t'+18t'^2)\right]\end{aligned} \tag{3.8}$$

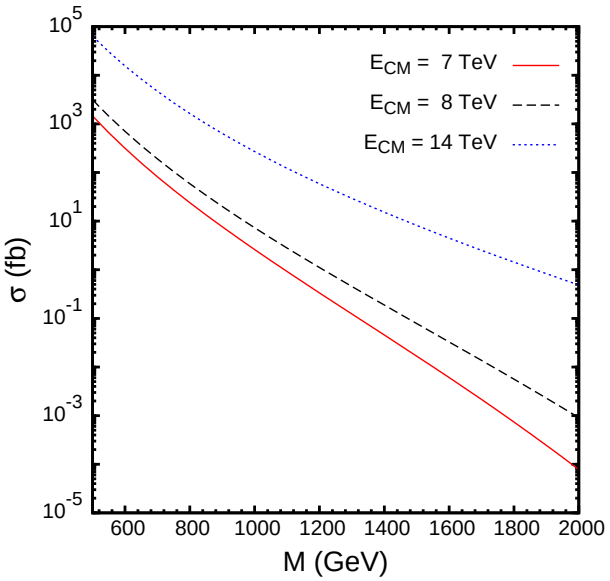

FIG. 2: *The production cross sections for* $pp \to Q_{3/2}\bar{Q}_{3/2}$ *at the LHC as a function of spin–*$\frac{3}{2}$ *quark mass* M *at center-of-mass energies,* $E_{CM} = 7, 8$ *and* 14 *TeV. We have chosen the scale as* $Q = M$*, the mass of the spin–*$\frac{3}{2}$ *quark.*

and the total cross section for this subprocess is

$$\hat{\sigma}(q\bar{q} \to Q_{3/2}\bar{Q}_{3/2}) = \frac{\pi\alpha_s^2}{81\hat{s}}\beta\left[\frac{8}{3}y^2 - \frac{16}{3}y - \frac{16}{3} + 96\frac{1}{y}\right] . \tag{3.9}$$

To obtain the production cross section we convolute Eq.(3.6) and Eq.(3.9) with the parton distribution functions (PDF).

$$\begin{aligned}\sigma(pp \to Q_{3/2}\bar{Q}_{3/2}) = &\left\{\sum_{i=1}^{5}\int dx_1 \int dx_2\ \mathcal{F}_{q_i}(x_1, Q^2) \times \mathcal{F}_{\bar{q}_i}(x_2, Q^2) \times \hat{\sigma}(q_i\bar{q}_i \to Q\bar{Q})\right\} \\ &+ \int dx_1 \int dx_2\ \mathcal{F}_g(x_1, Q^2) \times \mathcal{F}_g(x_2, Q^2) \times \hat{\sigma}(gg \to Q\bar{Q}),\end{aligned} \tag{3.10}$$

where $\mathcal{F}_{q_i}$, $\mathcal{F}_{\bar{q}_i}$ and $\mathcal{F}_g$ represent the respective PDF's for partons (quark, antiquark and gluons) in the colliding protons, while Q is the factorization scale. In Fig.2 we plot the leading-order production cross section for the process $pp \to Q_{3/2}\bar{Q}_{3/2}$ at center of mass energies of 7, 8 and 14 TeV as a function of the spin–$\frac{3}{2}$ quark mass M. We set the factorization scale Q equal to M, and used the `CTEQ6`ℓ`1` parton distribution functions [15]. This production cross section is larger than any spin-$\frac{1}{2}$ colored fermion of same mass such as a fourth-generation quark or an excited quark. This is not unexpected, as the cross section

given in Eq.(3.6) grows with energy as $\hat{s}^3$ which violates unitarity at high energies. We assume that the interactions given in Sec.II represent an effective interaction such that, at higher energies, higher order contributions will be important and the cross section will be damped by some form factors dependent on the scale of the new physics. Some explicit ways to address this have been discussed in Refs.[10, 16]. There is some natural enhancement, however, because the particles carry additional spin degree of freedom when compared to spin-$\frac{1}{2}$ fermions.

We find that for the 7 TeV run of the LHC, the pair production of a colored spin–$\frac{3}{2}$ exotic fermion has cross sections in excess of a few hundred femtobarns (fb) for masses as high as 600 GeV. At the current run of the LHC, with a center of mass energy of 8 TeV, cross sections in excess of 100 fb are obtained for masses up to 750 GeV. Therefore a strong case can be made to search for such exotics in the current and upcoming LHC data, just as that being done for coloron like particles.

Any search for these exotics would crucially depend on how the particle decays and what is produced in the final state so let us now discuss how these particles will decay. Higher dimension-five operators would lead to interactions between the massive spin–$\frac{3}{2}$ states and the spin–$\frac{1}{2}$ states such as [10]

$$\mathcal{L}_{dim-5} = i\frac{g_s}{\Lambda}\bar{\psi}_\alpha \left(g^{\alpha\beta} + A\gamma^\alpha\gamma^\beta\right)\gamma^\nu T^a \frac{(1\pm\gamma_5)}{2}\xi F^a_{\beta\nu} + H.C. \tag{3.11}$$

where $F^a_{\beta\nu}$ represents the field tensor of the gauge field and ξ is the spin–$\frac{1}{2}$ fermion. Λ determines the scale of some new physics which, for example, could be the scale which remedies the unitarity violation seen in the cross section. Note that large values of scale Λ would imply that the interaction strength weakens. We will assume that the colored spin–$\frac{3}{2}$ will decay promptly to a gluon and a spin–$\frac{1}{2}$ fermion (which in our case is a SM quark) with 100% branching probability. So there is no need for us to calculate a branching ratio and thus no need to use Eq.(3.11). The only thing we need is for Λ to be large enough such that Eq.(3.11) does not change the production cross section significantly. However, the scale Λ if accessible at LHC energies would lead to new physics signals. In our work we have assumed that this scale is large and inaccessible at the current run of LHC.

Thus if the quantum numbers dictate a decay to a particular family of quarks we can have three different scenarios corresponding to the decay of the spin–$\frac{3}{2}$ particle to one of the three SM quark families, a light SM quark and a gluon ($Q_{3/2} \to qg$), or a heavy quark

and a gluon ($Q_{3/2} \to bg$ or $Q_{3/2} \to tg$). We will now analyze each of these signals and the corresponding SM background representative of the type of decay. It is worth pointing out here that all our calculations are at leading-order and subsequent analysis are based on leading-order parton level analysis.

IV. SIGNALS AT THE LHC

A. Four jet final state

As mentioned above we assume that the spin–$\frac{3}{2}$ colored fermion can decay to a SM quark and a gluon. If the quark happens to belong to the first two families of the SM quarks, then these quarks will hadronize and form jets, as will the gluons, leading to four jets in the final state. All the jets will carry large transverse momenta (p_T) as they are byproducts of a heavy particle decay. However, with final states only comprised of jets the signal will be overwhelmed by the huge QCD background which would also be characterized by high p_T jets. Therefore to extract the signal from the huge background, one needs to devise some specific conditions on the kinematics of the final state particles and also put the focus on to the uniqueness of the signal coming from the new particles. The most obvious feature that the signal will exhibit is a peak in the invariant mass distribution of a pair of jets coming from the decay of the spin–$\frac{3}{2}$ quark. In comparison, the QCD background would trail off for high invariant mass values of the dijet. This signal could be mimicked by other new physics scenarios where new colored particles produced in pairs decay hadronically to dijets. In fact the CMS Collaboration has made an initial analysis on such particles at LHC with $\sqrt{s} = 7$ TeV using 2.2 fb^{-1} of integrated luminosity and put a lower limit on the mass of coloron-type particles to be 580 GeV [18]. We have used the CMS analysis to obtain an effective lower limit of $M \sim 490$ GeV on the mass of a spin–$\frac{3}{2}$ quark which decays into a light quark and gluon. Note that the bound is lower than the coloron mass bound because for similar masses the pair production cross section for spin–$\frac{3}{2}$ quarks is smaller than the pair production of colorons.

The search strategies at CMS did not include stronger cuts on the p_T of the jets, which should further suppress the large QCD background for the $4j$ final state. In Table I we summarize the signal cross section with different set of p_T cuts on the jets in the final state

and also highlight how the cuts affect the QCD background. In addition to the p_T cut, the jets must lie within the rapidity gap of $|\eta_j| < 2.5$ and the jets are isolated in the (η, ϕ) plane satisfying $\Delta R_{jj} > 0.5$, where ΔR is defined as $\Delta R = \sqrt{(\Delta\eta)^2 + (\Delta\phi)^2}$. A minimum cut on the invariant mass of each dijet pair has been also implemented for both signal and background, given by $M_{jj} > 10$ GeV. As one would expect, for stronger requirements on the jet p_T, the QCD background begins to fall off rapidly. The signal is affected more by the p_T cuts for smaller values of the spin–$\frac{3}{2}$ quark mass because the jets have higher p_T if they come from the decay of heavier spin–$\frac{3}{2}$ quark. The numbers in Table I demonstrate this, as stronger cuts are shown to effect the background more by suppressing it at times by more than 90% which improves the signal to background ratio significantly. Thus with 2.2 fb^{-1} integrated luminosity(L) at $\sqrt{s} = 7$ TeV, and a p_T cut of 200 GeV, we find that the ratio of signal to square root of background, $S/\sqrt{B} \equiv L\sigma_s/\sqrt{L\sigma_b}$ is about 4.4 for a spin–$\frac{3}{2}$ quark

	Signal cross-section (fb)						
	M (GeV)						
$\boldsymbol{p_T}$ cut (GeV)	500	600	700	800	900	1000	SM background (fb)
	$\boldsymbol{\sqrt{s} = 7}$ **TeV**						
200	326.	124.	48.6	18.8	7.2	2.8	11900.
250	134.	51.9	24.9	11.5	5.1	2.1	2420.
300	65.2	21.0	10.1	5.7	3.0	1.5	577.
	$\boldsymbol{\sqrt{s} = 8}$ **TeV**						
300	194.	61.2	27.6	15.1	8.1	4.1	1270.
350	106.	32.2	12.6	6.6	4.1	2.4	377.
400	58.1	17.6	6.5	3.0	1.8	1.2	118.
	$\boldsymbol{\sqrt{s} = 14}$ **TeV**						
400	4842.	1549.	569.4	242.2	120.8	69.7	3013.
450	3271.	1074.	399.7	167.6	79.5	43.3	1315.
500	2184.3	746.9	280.8	117.6	54.9	28.4	609.2

TABLE I: *The signal cross section for the $4j$ final state coming from the pair production of spin–$\frac{3}{2}$ quarks of mass M with $\sqrt{s} = 7, 8$ and 14 TeV as the cut on the transverse momenta of the jets is varied. Also shown is the QCD background which has been estimated using* Madgraph *5 [17].*

with mass $M = 500$ GeV which suggests a significant improvement in the mass reach for such exotic particles. At $\sqrt{s} = 7$ TeV, the stronger cuts are not helpful as they also suppress the signal by a large amount.

It is worth pointing out here that our analysis, done at the leading-order parton level, does not correspond to the exact numbers seen at the experiments as no detector level effects have been included. However, after accounting for the suppression in events due to hadronization and fragmentation effects, detector efficiencies and acceptance, the strong cuts would still help in improving the mass reach for colored particles which are pair produced and decay hadronically to a pair of jets.

B. Final state with two b–jets and two light jets

In this section we consider the scenario where the spin–$\frac{3}{2}$ quark quantum numbers dictate its decay to a bottom quark and a gluon so the pair produced spin–$\frac{3}{2}$ quarks lead to a final state with two b-jets and two light jets ($2b2j$) all carrying large transverse momenta. This final state is already included in the $4j$ analysis when no heavy flavor tagging is applied on the events. However, recent analysis at both ATLAS and CMS have shown that a very high efficiency for b-tagging may be obtained [19, 20]. Dependent on the transverse momenta of the b-jets, the efficiencies could be as high as 70% for jets with $p_T > 100$ GeV. So even though we lose part of the events due to limited efficiencies, the QCD background is reduced significantly as the b-jet production forms a small subset of the full $4j$ background. On the other hand, the pair production cross section for the spin–$\frac{3}{2}$ quark remains unaffected even if its quantum numbers correspond to a bottom quark. Therefore, the signal events will benefit from such flavor tagging and improve the signal to background ratio.

In Fig.3 and Fig.4 we plot the invariant mass distribution of the two final state jets with the leading b-jet. Note that in the analysis for a resonant particle, the resonance is not seen in the two b-jet invariant mass but is seen in the light quark jet and b-jet. This will reduce the QCD background significantly. We plot the invariant mass distribution for three different values of the spin–$\frac{3}{2}$ quark mass and at three different center of mass energies. Both the light quark jets and the b-jets are ordered according to their p_T and we call the leading b-jet as b_1 and the subleading b-jet as b_2 with similar notation for the light quark jets. The

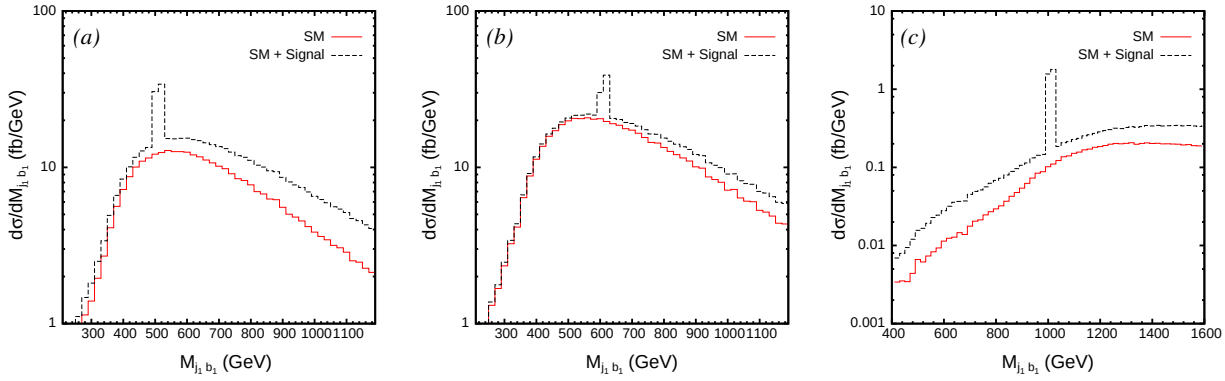

FIG. 3: *The invariant mass distribution of the leading jet and leading b-jet for the SM background and the superposed signal coming from the production of spin–$\frac{3}{2}$ quarks with the SM background. Distributions are shown for three different values of mass of the spin–$\frac{3}{2}$ quark and at different center of mass energies, viz. (a) $M = 500$ GeV; $\sqrt{s} = 7$ TeV, (b) $M = 600$ GeV; $\sqrt{s} = 8$ TeV and (c) $M = 1$ TeV; $\sqrt{s} = 14$ TeV.*

events used in the plots presented in Fig.3 and Fig.4 for both the signal and the background satisfy the following kinematic selection cuts:

- Both the light quark jets and b-jets have a minimum transverse momenta $p_T > 150$ GeV and lie within the rapidity gap of $|\eta| < 2.5$.

- To resolve the final states in the detector they should be well separated. To achieve this we require that they satisfy $\Delta R_{ij} > 0.7$ with i, j representing the b-jets and the light quark jets. As above the variable ΔR_{ij} defines the separation of two particles in the (η, ϕ) plane of the detector with $\Delta R_{ij} = \sqrt{(\eta_i - \eta_j)^2 + (\phi_i - \phi_j)^2}$, where η and ϕ represent the pseudo-rapidity and azimuthal angle of the particles respectively.

- To suppress large contributions of gluon splitting into two (b) jets we demand that the minimum invariant mass of two (b)-jets satisfy $M_{ij}^{inv} > 10$ GeV.

- We also demand that there are no additional jets with $p_T > 150$ GeV.

A clear resonance is observed in both the $M_{j_1 b_1}$ and $M_{j_2 b_1}$ distributions in the bin corresponding to the spin–$\frac{3}{2}$ quark mass. It is interesting to observe that both the leading and subleading jet forms a resonance in the invariant mass with the leading b-jet. As we have ordered the jets according to their p_T, their respective points of origin become immaterial

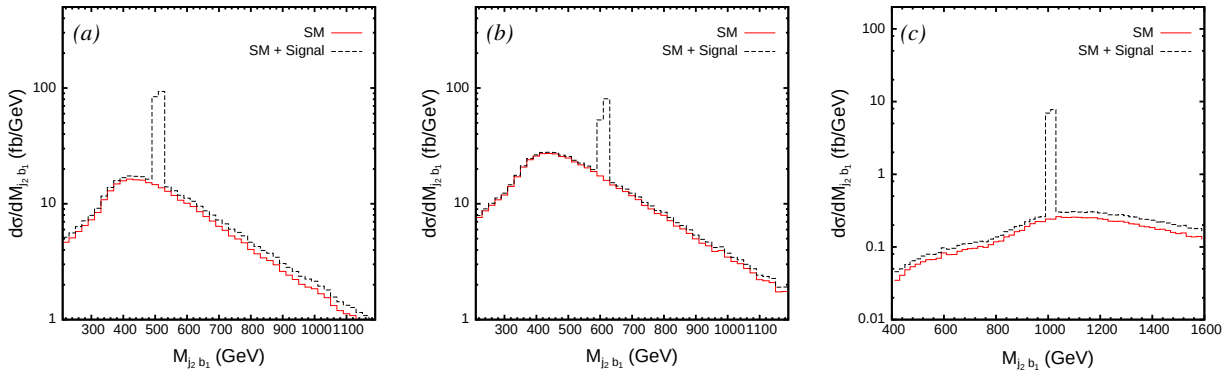

FIG. 4: *The invariant mass distribution of the sub-leading jet and leading b-jet for the SM background and the superposed signal coming from the production of spin–$\frac{3}{2}$ quarks with the SM background. The choices of M and $\sqrt{s}$ are the same as in Fig.3.*

and therefore both the combinations show an invariant mass peak. However, the subleading jet gives the more pronounced peak with the leading b-jet which seems to make it the favorable combination.

We have used three different values for the spin–$\frac{3}{2}$ quark mass, $M = 500$ GeV, 600 GeV, and 1 TeV at $\sqrt{s} = 7, 8$ and 14 TeV respectively. As the larger center of mass energy gives a bigger pair production cross section (Fig.2), we choose larger values for the spin–$\frac{3}{2}$ quark mass for higher $\sqrt{s}$ to show that the signal will be significantly greater even for the larger values of mass which are inaccessible with lower center of mass energies. We use the same set of kinematic cuts for the analysis done at $\sqrt{s} = 7$ and 8 TeV. However, as in the case of $4j$ final states, stronger cuts on the transverse momenta of both the b-jet and the light quark jet would be useful in improving the signal to background ratio. We therefore modify the cut on transverse momenta and demand that $p_T > 400$ GeV for the jets at $\sqrt{s} = 14$ TeV. For our analysis of both the signal and background, we have considered a b-tagging efficiency of 50% while the mistag rate for light quark jets tagged as b-jets is taken as 1%. Both the b-tag efficiency and the mistag rates are dependent on the transverse momenta (p_T) and rapidity (η) and our choices do not include these effects. To do such detailed analysis one would also need to include various other systematics including showering and hadronization effects at the LHC and detector-level simulations which is beyond the scope of this work. So we assume that our choice for the efficiencies and the mistag rate is a good approximation when averaged over the entire range of transverse momenta for the quarks

within the allowed rapidity gap.

With the above set of cuts the signal cross section for different values of the spin–$\frac{3}{2}$ mass along with the SM background are shown in Table II. When compared with $4j$ analysis, the reach for spin–$\frac{3}{2}$ quarks in the $2b2j$ channel is found to be improved significantly. For example, for $M = 1$ TeV with an integrated luminosity of 10 fb^{-1} for $\sqrt{s} = 14$ TeV and a $p_T > 400$ GeV cut on the jets, the $S/\sqrt{B} \simeq 4$ in the $4j$ final state while it becomes $S/\sqrt{B} \simeq 15$ in the $2b2j$ final state.

$pp \to 2b2j$	Signal cross-section (fb)						SM background (fb)
	M (GeV)						
	500	600	700	800	900	1000	
$\sqrt{s} = 7\ TeV$	182.5	55.0	17.6	5.9	2.1	0.7	351.3
$\sqrt{s} = 8\ TeV$	403.0	124.8	41.6	14.7	5.5	2.1	608.9
$\sqrt{s} = 14\ TeV$	584.8	275.4	123.4	57.6	29.7	17.1	12.9

TABLE II: *The signal cross section for the $2b2j$ final state at LHC with $\sqrt{s} = 7, 8$ and 14 TeV for different choices of the mass M. Note that the p_T cut on the jets is 150 GeV for $\sqrt{s} = 7$ and 8 TeV while it is 400 GeV for $\sqrt{s} = 14$ TeV. We have included a b-tag efficiency $\epsilon_b = 0.5$ in cross sections.*

C. Final state with $t\bar{t}$ and two light jets

Finally we specialize to the case where the spin–$\frac{3}{2}$ quark carries quantum numbers similar to the top quark and therefore decays to a top quark and a gluon. This would lead to a $t\bar{t}$ final state with two additional jets with large transverse momenta through the process chain given by $pp \longrightarrow Q_{3/2}\bar{Q}_{3/2} \longrightarrow t\bar{t}gg$.

This would be a very nice signal which would not only provide a strong hint for physics beyond the SM but would also effect the inclusive top quark pair production if the additional jets are not triggered upon. However, as the production cross section of the heavier $Q_{3/2}$ particles are small compared to the pair production of $t\bar{t}$ (about 10% of $\sigma_{t\bar{t}}$ for $M = 400$ GeV) the new physics signal is more pronounced when the additional jets with high p_T are triggered on. We look at the $t\bar{t}jj$ signal and SM background and consider a 100 GeV

$pp \to t\bar{t}jj$ ($p_T^j > 100$ GeV)	Signal cross-section M (GeV) 500	800	1000	SM background
$\sqrt{s} = 7\ TeV$	1.11 pb	21.7 fb	2.4 fb	2.12 pb
$\sqrt{s} = 8\ TeV$	2.38 pb	53.4 fb	6.8 fb	3.55 pb
$\sqrt{s} = 14\ TeV$	49.4 pb	1.46 pb	249. fb	24.7 pb

TABLE III: *The signal cross section for the $t\bar{t}jj$ final state coming from the pair production of spin–$\frac{3}{2}$ quarks with $\sqrt{s} = 7, 8$ and 14 TeV for different choices of the mass M for a fixed cut of 100 GeV on the transverse momenta of the jets. Also shown is the dominant QCD background in SM which has been estimated using* `Madgraph 5`.

cut on the transverse momenta of the additional (nontop) jets. Note that by demanding two jets with $p_T > 100$ GeV along with a $t\bar{t}$ pair would completely eliminate the large background coming from the pair production of $pp \to t\bar{t}$. We generate the SM background using `MadGraph 5` for $pp \to t\bar{t}jj$ and $pp \to t\bar{t}jj(+j)$ with some additional basic acceptance cuts of $|\eta_j| < 2.5$ and $\Delta R_{jj} > 0.5$. We list the cross section for the signal and background for different values of the spin–$\frac{3}{2}$ quark mass in Table III.

A quick comparison of the signal with the background shows that the although the background is quite large when compared to the signal for $M = 1$ TeV, our experience from the previous analysis of $4j$ and $2b2j$ signal implies that stronger cuts on the transverse momenta of the jets will suppress the background further. As before the signal will not change much for large values of M.

To put this in perspective let us now consider the full decay of the top quarks in the final state and look more closely at the signal and SM background for two different set of cuts on the transverse momenta of the jets. To analyze the signal we focus on the semileptonic decay mode of the produced top quark leading to the following final state:

$$\begin{aligned} pp \longrightarrow & (Q_{3/2} \to tg) \longrightarrow (t \to bW^+)g \longrightarrow (W^+ \to \ell^+\nu_\ell)bg \\ \hookrightarrow & (\bar{Q}_{3/2} \to \bar{t}g) \longrightarrow (\bar{t} \to \bar{b}W^-)g \longrightarrow (W^- \to \ell^-\bar{\nu}_\ell)\bar{b}g \\ \hookrightarrow & \ell^+\ell^- b\bar{b}jj\not{E}_T \end{aligned} \tag{4.1}$$

where we restrict ourselves to the choice of $\ell = e, \mu$ for the charged lepton. As it is very

difficult to differentiate between b and $\bar{b}$ even with heavy flavor tagging of the jets, we are looking at a final state with a pair of charged leptons ($\ell_i^+\ell_j^-$), two hard b-jets, two hard light quark jets and missing transverse momenta. We define two set of cuts which we list in Table IV. The results in Table V show that going from the cuts $\mathcal{C}_1$ to the cuts $\mathcal{C}_2$ drastically reduces the background without much change in the signal.

The conclusions to be drawn from Table V are the following: 1) at $\sqrt{s} = 8$ TeV the p_T cuts extend the reach above $M = 500$ GeV but well below $M = 800$ TeV the signal cross-section becomes too small to be observed (independent of the cuts). 2) At $\sqrt{s} = 14$ TeV the stronger p_T cuts seem unnecessary for M near 500 GeV but become essential for M equal 800 GeV. At $M = 1000$ GeV the cross-section is small but could be seen when the integrated luminosity exceeds about 200 fb^{-1}.

V. DISCUSSION AND SUMMARY

In this work we have focused on the signals for colored spin–$\frac{3}{2}$ fermions at the LHC. These particles will have large production cross sections and can be discovered through resonances in different channels depending on their decay properties. We have presented complete analytic expressions for the parton-level matrix amplitudes and cross sections used in our calculations.

We considered three different scenarios for the higher spin fermion mixing with SM quarks

Variable	Cut $\mathcal{C}_1$	Cut $\mathcal{C}_2$
$p_T^{\ell,b}$	$> 10, 20$ GeV	$> 10, 20$ GeV
$\boldsymbol{p_T^j}$	> 50 GeV	> 200 GeV
$\lvert\eta\rvert$	< 2.5	< 2.5
$\boldsymbol{\Delta R_{jj}}$	> 0.4	> 0.7
$\Delta R_{\ell\ell,\ell j,\ell b,bj}$	> 0.2	> 0.2

TABLE IV: *Two different set of cuts $\mathcal{C}_1$ and $\mathcal{C}_2$, imposed on the final state $\ell^+\ell^- bbjj\not{E}_T$ where the cuts are different only on the kinematic variables shown in bold. Not listed is a b-tagging efficiency of $\epsilon_b = 0.5$ for both sets.*

$pp \to \ell^+\ell^- bbjj\not{E}_T$	Signal cross-section (fb)			SM background (fb)
	M (GeV)			
	500	800	1000	
$\sqrt{s} = 8\ TeV$	20.1 (7.8)	0.4 (0.3)	0.055 (0.045)	93.2 (2.9)
$\sqrt{s} = 14\ TeV$	385.9 (186.1)	11.2 (8.2)	1.9 (1.6)	522.8 (26.7)

TABLE V: The signal cross section for the $\ell^+\ell^- bbjj\not{E}_T$ final state with $\sqrt{s} = 8$ and 14 TeV for different choices of the mass M for the cuts $\mathcal{C}_1(\mathcal{C}_2)$ shown in Table IV.

which dictates the decay modes. We find that such an exotic fermion can decay hadronically to two light jets or into a gluon and heavy quark flavors. This leads to three different final state topologies $4j$, $2b2j$ and $t\bar{t}jj$. We did a detailed analysis of the three different cases and show that a strong cut on the transverse momenta of the final state jets is very useful in suppressing the otherwise large QCD background for hadronic final states at LHC. We have compared our results with a CMS study on $4j$ final states and extracted a lower bound of 490 GeV on the spin–$\frac{3}{2}$ quark mass. We further showed that this reach can be improved by using stronger cuts on the p_T of the jets; the details are given in Table I. Given that only a limited amount of luminosity will be collected at $\sqrt{s} = 8$ TeV the reach in M for this final state is between 600 GeV and 700 GeV. At $\sqrt{s} = 14$ TeV the reach easily exceeds $M = 1$ TeV.

We then considered the case where the spin–$\frac{3}{2}$ quark decays to a gluon and a bottom quark and showed, in Figs. 3 and 4, that the event characteristics of such a final state leads to a clear invariant mass peak when the b-jet is paired with the gluon jets. We also showed, in Table II, that the SM background is suppressed in this final state which would lead to a better reach for spin–$\frac{3}{2}$ quark mass.

Finally we focused on the signal where the spin–$\frac{3}{2}$ quark decays to a top quark and gluon where the signal and background are shown, for nominal cuts, in Table III. The background for a top pair with two additional radiated gluons is seen to be large. However, as shown in Table V, this background can be greatly reduced by appropriate cuts which include a strong p_T requirement on the jets. For $\sqrt{s} = 14$ TeV these cuts extend the observation reach to $M = 1000$ GeV.

Acknowledgments

This research was supported in part by the United States Department of Energy under grants No. DE-FG02-04ER41306 and No. DE-FG02-12ER41830.

---

[1] S. Chatrchyan *et al.* [CMS Collaboration], Phys. Lett. B [arXiv:1207.7235 [hep-ex]].

[2] G. Aad *et al.* [ATLAS Collaboration], [arXiv:1207.7214 [hep-ex]].

[3] J.G. Taylor, Phys. Lett., **88B**, 291 (1979), and references therein; J.G. Taylor, Phys. Lett., **90B**, 143 (1979), and references therein.

[4] I. Antoniadis, Phys. Lett. **246B**, 377 (1990); I. Antoniadis, K. Benakali and M. Quiros, Phys. Lett. **331B**, 313 (1994); J. D. Lykken, Phys. Rev. **D54**, 3693 (1996); I. Antoniadis, S. Dimopoulos and G. Dvali, Nucl. Phys. **B516**, 70 (1998); K. R. Dienes, E. Dudas and T. Gherghetta, hep-ph/9803466; N. Arkani-Hamed, S. Dimopoulos and G. Dvali, hep-ph/9803315; A. Pomerol and M. Quiros, hep-ph/9806263.

[5] B. Moussallam and V. Soni, Phys. Rev. **D39**, 1883 (1988).

[6] D. A. Dicus, S. Gibbons and S. Nandi, hep-ph/9806312.

[7] R. Walsh and A. J. Ramalho, Phys. Rev. D **60**, 077302 (1999) [hep-ph/9907364].

[8] F. M. L. Almeida, Jr., J. H. Lopes, J. A. Martins Simoes and A. J. Ramalho, Phys. Rev. D **53**, 3555 (1996) [hep-ph/9509364].

[9] O. Cakir and A. Ozansoy, Phys. Rev. D **77**, 035002 (2008) [arXiv:0709.2134 [hep-ph]].

[10] W. J. Stirling and E. Vryonidou, JHEP **1201**, 055 (2012) [arXiv:1110.1565 [hep-ph]].

[11] W. Rarita and J. Schwinger, Phys. Rev. **60**, 61 (1941).

[12] P.A. Moldauer and K.M. Case, Phys. Rev. **102**, 279 (1956); S.C. Bhargava and H. Watanabe, Nucl. Phys. **87**, 273 (1966).

[13] V. Pascalutsa, hep-ph/9412321, HU-94-21.

[14] B. Moussallam, private communication. We thank Professor Moussallam for resolving this discrepancy.

[15] J. Pumplin, D. R. Stump, J. Huston, H. L. Lai, P. M. Nadolsky and W. K. Tung, JHEP **0207**, 012 (2002) [hep-ph/0201195].

[16] B. Hassanain, J. March-Russell and J. G. Rosa, JHEP **0907**, 077 (2009) [arXiv:0904.4108

[hep-ph]].

[17] J. Alwall et. al., J. High Energy Phys. 06 (2011) 128.

[18] V. Khachatryan et. al. [CMS Collaboration], Report No. CMS-EXO-11-016 (2011).

[19] ATLAS Collaboration, *Calibrating the b-tag efficiency and mistag rate in 35 pb^{-1} of data with the ATLAS detector*, **ATLAS-CONF-2011-089 (2011)**; *Identification and Tagging of Double b-hadron jets with the ATLAS Detector*, **ATLAS-CONF-2012-100 (2012)**.

[20] CMS Collaboration, *b-Jet Identification in the CMS Experiment*, **PAS-BTV-11-004 (2011)**.